Climate Dynamics (2024) 62:9377–9390
https://doi.org/10.1007/s00382-024-07400-1

ORIGINAL ARTICLE

Amazon drought amplifies SST warming in the North Tropical Atlantic

Wei Lou[1] · Cheng Sun[1] · Fred Kucharski[2] · Jianping Li[3,4] · Yusen Liu[1]

Received: 23 March 2024 / Accepted: 7 August 2024 / Published online: 27 August 2024

Abstract
North Tropical Atlantic (NTA) has been warming rapidly in the winter, with a warming rate that exceeds the global average sea surface temperature (SST). However, the reasons for this enhanced warming remain unclear. Here we suggest that Amazon drought contributes to the rapid NTA warming. Observational analyses reveal that Amazon Soil Moisture (ASM) in autumn shows a significant inverse relationship with NTA SST in winter. Decreased ASM in autumn, persists via Land-Atmosphere (L-A) feedback, leads to weakened Hadley circulation over the Tropical Atlantic in winter. The Wind-Evaporation-SST (WES) feedback mechanism further causes the warming of NTA SST. Simulations from CMIP6 fully coupled models and SM-forced mixed layer ocean model suggest that the Amazon drought weakens the Hadley circulation over the Tropical Atlantic and warms the NTA SST. An ASM-based empirical model reproduces the observed NTA SST variations ($r=0.72$, $p<0.05$), further highlighting a role for Amazon drought in amplifying ocean warming.

Keywords North Tropical Atlantic · Amplified SST warming · Amazon drought · Local hadley circulation · Land-atmosphere-ocean interactions

1 Introduction

The North Tropical Atlantic (NTA) Sea Surface Temperature (SST) anomaly exerts a significant impact on the climate variability over the surrounding areas(Ham et al. 2013; Huo et al. 2015; Wang et al. 2006). It can induce alterations in the formation and paths of tropical cyclones and hurricanes and affect the spatial distribution of precipitation and temperature in the Northern Hemisphere(Chen et al. 2020; Jin and Huo 2018). The warming of NTA SST is mainly forced by El Niño-Southern Oscillation (ENSO) and North Atlantic Oscillation (NAO), driven and sustained by the Wind-Evaporation-SST (WES) feedback mechanism, and related to the latent heat flux anomalies caused by weakening of the northeast trade winds(Chang et al. 1997; Czaja et al. 2003; Jiang and Li 2019). ENSO triggers the Pacific-North American (PNA) pattern(Enfield and Mayer 1997), inducing tropospheric heating(Chang et al. 2006) and anomalies in the Hadley circulation(Wang 2004). This leads to reduced evaporation and latent heat flux from the ocean surface, causing anomalous warming of the NTA SST. On the other hand, the negative phase of the NAO weakens the subtropical high, inducing anomalous southwesterlies over the NTA. Consequently, this weakens the northeast trades, reduces upward latent heat flux from evaporation, and contributes to the anomalous warming of SST(Czaja et al. 2003). As mentioned above, previous studies on NTA warming have primarily focused on oceanic and atmospheric factors, such as ENSO and NAO, while paying little attention to the role of Land-Atmosphere (L-A) coupling factors.

Soil Moisture (SM) is a key factor for L-A coupling(Seneviratne et al. 2006; Song et al. 2019; Yang et al. 2018a). The interaction between SM and the atmosphere, known as Soil Moisture-Atmosphere (SM-A) feedback, has significant impacts on various climatic factors, including air

✉ Cheng Sun
scheng@bnu.edu.cn

1 State Key Laboratory of Remote Sensing Science, Faculty of Geographical Science, Beijing Normal University, Beijing 100875, China

2 Abdus Salam International Centre for Theoretical Physics, Trieste, Italy

3 Frontiers Science Center for Deep Ocean Multi-Spheres and Earth System (DOMES)/Key Laboratory of Physical Oceanography/Academy of Future Ocean/College of Oceanic and Atmospheric Sciences/Center for Ocean Carbon Neutrality, Ocean University of China, Qingdao 266100, China

4 Laoshan Laboratory, Qingdao 266237, China

temperature, precipitation, atmospheric boundary layer stability, and even large-scale atmospheric circulation anomalies. This influence extends beyond local areas, as changes in SM can impact surface energy balance and water vapor transport, thereby influencing atmospheric conditions on a larger scale(Cook et al. 2006; Eltahir 1998; Seneviratne et al. 2010; Yang et al. 2018a). The impact of SM variability and its role in L-A coupling is particularly pronounced in regions known as hotspots(Qiao et al. 2021). One such hotspot is the Amazon rainforest, rich in soil water content, one of the largest tropical rainforests and strongest L-A coupling regions in the world, that is adjacent to the NTA ocean. The active high evapotranspiration in the Amazon rainforest modulates local atmospheric water cycle and energy balance, consequently impacting atmospheric circulation pattern(Lejeune et al. 2015; Nobre et al. 2009). In recent decades, Amazon rainforest has faced significant drought risks, primarily due to large-scale deforestation caused by human activities(Nobre et al. 2016). SM serves as a crucial indicator of drought conditions in the Amazon, as it reflects the availability of water in the soil, which directly affects plant growth and vegetation in the rainforest. Understanding the local climate impact of deforestation and drought in the Amazon is one of the primary focuses of the current literature. For example, deforestation in the Amazon leads to surface temperature warming and drought(Alves de Oliveira et al. 2021), diminishing the rainforest's ability to sequester carbon and potentially turning them into carbon sources(Gatti et al. 2021). Moreover, the decreased SM in the Amazon inhibits evaporation, resulting in higher temperatures(Geirinhas et al. 2022) and impacting carbon flux (Levine et al. 2019). However, the remote effects of the Amazon rainforest, especially on the ocean, remain a significant gap in the literature. Considering the geographic proximity between the Amazon rainforest and the NTA, the influence of the Amazon rainforest changes on the NTA remains undetermined and warrants further investigation.

Recent research has emphasized the significant impact of atmospheric and oceanic factors on the NTA SST anomaly(Amaya et al. 2017; Yang et al. 2018b). However, the influence of land surface factors on SST variability remains poorly understood in the existing literatures. Meanwhile, Amazon rainforest, neighboring the NTA, has experienced frequent drought events(Boulton et al. 2022; Jiménez-Muñoz et al. 2016). The change in atmospheric circulation caused by variations in Amazon Soil Moisture (ASM) is likely to induce changes in NTA SST through land-atmosphere-ocean interaction. Studying the impact of ASM on NTA SST variability will provide a novel perspective on the role of SM, a land-atmosphere factor, in SST variability. This will contribute to a more comprehensive understanding of the mechanisms and characteristics of SST variability, enhance our comprehension and predictive capacity concerning climate change, and facilitate a better understanding of the interactions and impacts between crucial ecosystems and marine systems, thus enabling improved forecasts of future climate change and ecosystem shifts.

2 Data and method

2.1 Data

In this study, the sea surface temperature data is derived from Extended Reconstructed SST version 5 (available at https://psl.noaa.gov/data/gridded/data.noaa.ersst.v5.html) (Huang et al. 2017). The atmospheric data for sea level pressure, precipitation, vertical velocity, surface winds are derived from the ECMWF reanalysis, ERA5(Hersbach et al. 2020). Compared with the previous versions, the ERA5 product shows a significant improvement in representing the variability and magnitude of near-surface air temperature and wind fields. The surface heat flux data are also derived from the ERA5 product, and the latent heat flux is defined to be positive upward in this study. All data are employed and analyzed for the period 1983–2019.

The monthly soil moisture data for global terrestrial surfaces is derived from the Terra Climate(Abatzoglou et al. 2018), which is a combination of the CRU TS climate data set (Climatic Research Unit gridded Time Series) World Climdata set and the JRA data set (available at wwwclimatologylab.org/terraclimate.html). The Terra Climate dataset is based on station and reanalysis data and is available from 1958 to present. The dataset has a rather high resolution at 4 km, which is then conformed to T63 grids ($1.88° \times 1.88°$) to match the resolution of atmospheric data. We also use the top layer of soil moisture dataset from ERA5 for complementary validation. To describe the drought, we also use the Palmer Drought Severity Index (PDSI)(Dai 2011) (available at https://climatedataguide.ucar.edu/climate-data/palmer-drought-severity-index-pdsi) as a supplement to soil moisture.

This study uses the historical simulation of coupled models of the Coupled Model Intercomparison Project Phase 6 (CMIP6), which is based on the historical atmospheric radiative forcing fields (e.g., greenhouse gases and volcanic aerosols, etc.). Table S1 summarizes the CMIP6 models used in this study (available at https://esgf-index1.ceda.ac.uk/search/cmip6-ceda/). In this study, only the first ensemble member (i.e., r1i1p1) run of each model is used and the analysis is performed for the period 1980–2014 for all models. A large number of ensemble members are provided by the CMIP6 project, which have different variant labels (a label constructed from 4 indices stored as a global attribute)

based on realizations (r), initialization (i), physics (p), and forcing (f) indices. These indices are used to identify each simulation of an ensemble contributed by a single model. This study selected the first available ensemble member of the historical simulation of each model, with a variant label of r1i1p1f1. Although a few of the CMIP6 models have more than one ensemble member, we use a single member (r1i1p1f1) for each model for fair comparisons. The use of a single run for each model assures an equal weight for different CMIP6 models and the model performance is evaluated based on the r1i1p1f1 run of different CMIP6 models.

2.2 Definitions of various indices

In this study, to describe the variability of SST in NTA, the NTA SST index is defined as the averaged SST in the region of (0°–15°N, 80°W–10°W) in the North Tropical Atlantic. The ASM index and APDSI index are defined as the averaged soil moisture and PDSI in the region of (5°S–5°N, 65°W–45°W) in the Amazon. The Niño3.4 index, the most commonly used index to represent ENSO intensity, is defined as the average of SST anomalies over the Niño3.4 region (5°S–5°N, 170°W–120°W). The NAO index is defined as the principal component (PC) time series of the first Empirical Orthogonal Function (EOF) of SLP anomalies over the Atlantic sector (0°–90°N, 90°W–30°E). The IOD index is defined as the SST anomaly differences between the western (10°S–10°N, 50°E–70°E) and southeastern (10°S–0°, 90°E–110°E) tropical Indian Ocean(Saji et al. 1999).

2.3 Experimental design

In this study, the numerical experiments are conducted using ICTPGCM model to isolate the atmospheric and oceanic response to the reduction of SM in Amazon. The atmospheric component called Simplified Parameterizations, Primitive-Equation Dynamics (SPEEDY) is an atmospheric general circulation model (AGCM) developed by ICTP (Kucharski et al. 2006). The SPEEDY is intermediate, which contains eight vertical levels and adopts a horizontal resolution of T30 (3.75° × 3.75° grid). The model includes basic components of physical parameterizations used in more complex GCMs, such as convection (a simplified mass flux scheme), large-scale condensation, clouds, short-wave radiation (two spectral bands), long wave radiation (four spectral bands), and vertical diffusion. The land surface model is coupled to the atmospheric component of the ICTPGCM, which allows for the exchange of energy, water, and momentum between the land and atmosphere. The model has certain simulation capabilities for climate and land surface physics process, which has been widely used in global climate change research(Gore et al. 2020).

This study employs a Slab Ocean Model (SOM) as the ocean component within the ICTPGCM (Kucharski et al. 2016). This choice aligns with prior findings (Foltz et al. 2013; Rugg et al. 2016) highlighting the dominant role of mixed-layer thermodynamics in driving NTA SST warming. Consequently, the SOM's focus on these processes renders it a well-suited and computationally efficient tool for SST simulation within this context. In the SOM, the depth (d0) of the mixed layer is constant throughout the whole simulation period, varying between 60 m (d0max) in the extra tropics and 40 m (d0min) in the tropics. The climatological annual-averaged mixed layer depth is geographically varying, generally shallow in the tropics and deep in mid-high latitudes. Besides, a heat flux correction is applied to climatological SST for the SOM and the mixed-layer temperature variation is derived from the integration of the net heat flux into the ocean (the sum of surface shortwave and longwave radiation and sensible and latent heat flux; all fluxes anomalies are defined as positive downward(Sun et al. 2017).

We designed two sets of experiments to isolate the climatic impact of decreased soil moisture: a control experiment (CTRL) and a sensitivity experiment (SM_Neg). In both experiments, prescribed soil moisture is imposed within a defined domain (5°S–5°N, 65°W–45°W) at each time step. Outside the domain, climatological monthly varying soil moisture is applied to the land surface to ensure that the difference in soil moisture between the two experiments was confined to the Amazon region, highlighting the impact of soil moisture drying in the Amazon. CTRL: The available soil moisture (both top soil layer and root zone) is prescribed using a monthly climatology. SM_Neg: The available soil moisture in the top soil layer is prescribed as the climatology superimposed with an anomaly term. This anomaly is defined as the product of the observed linear trend value, a 37-year time range (1983–2019) and a scaling factor. The difference between the SM_Neg and CTRL experiments isolates the climatic effect of decreased soil moisture over the Amazon region. The CTRL and SM_Neg experiment are integrated for 50 year of which the first 30 year are discarded. The scaling factor of five is used to make sure that the model produces steady and strong enough responses to the SM forcing with short integrations. The atmospheric and oceanic responses to the ASM forcing is defined as the difference between the ensemble means of the sensitivity and control runs scaled by a factor of 1/5.

2.4 Statistical analysis

To assess the statistical significance of differences in winter NTA SST following anomalously dry ASM conditions,

we employ a bootstrap resampling method (Austin and Tu 2004). The 15 values of the winter NTA SST anomaly index for wet autumn ASM anomaly (ASM anomaly > 5 mm) and 15 values of the winter NTA SST anomaly index for dry autumn ASM anomaly (ASM anomaly <−5 mm) in observations are resampled randomly to construct 10,000 realizations of the NTA SST anomaly index, respectively. We calculate the s.d of the 10,000 realizations of mean value for the two groups, and if the mean value difference between the two groups is greater than the sum of the doubled s.d. values, the difference is considered statistically significant above the 95% confidence level.

In this study, Multiple Linear Regression (MLR) statistical method(Krzywinski and Altman 2015) is used to determine the skill of the forcing factor to reproduce the NTA SST and to explain the contribution. MLR is widely used for analyzing the relationship between a dependent variable and two or more independent variables by fitting a linear equation. It has commonly employed in climate impact analysis (Folland et al. 2018). In this study, the ordinary linear least squares (LLS) regression is used to estimate the coefficients of the independent variables. LLS regression works by minimizing the sum of squares of residuals between observations and the predicted values obtained from the linear equation. MLR model can be written as [Eq. 1]:

$$Y = \beta_0 + \beta_1 X_1 + \beta_2 X_2 + \cdots + \beta_n X_n + \epsilon \tag{1}$$

where Y is the dependent variable, X_i are independent variables, β_i are parameters, ϵ is the error. The regression equation is estimated such that the total sum of squares (SST) can be partitioned into components due to regression (SSR) and residuals (SSE). The explanatory power of regression is summarized by the coefficient of determination R^2, which is ranges from 0 to 1 and calculated from the sum of squares terms [Eq. 2]:

$$R^2 = \frac{SSR}{SST} = 1 - \frac{SSE}{SST}$$

$$SST = \sum_{i=1}^{n}\left(Y_i - \bar{Y}_i\right)^2 \quad SSR = \sum_{i=1}^{n}\left(\hat{Y}_i - \bar{Y}_i\right)^2 \quad SSE = \sum_{i=1}^{n}\left(Y_i - \hat{Y}_i\right)^2 \tag{2}$$

In this study, we also use common statistical methods such as regression analysis, correlation analysis, and partial correlation analysis. Using the least square method(Agami Reddy 2011), we calculate the linear trends of time series. Using the Theil-Sen trend estimation method(Sen 1968), we calculate the trends of data. Since the data used in this paper are all monthly data, the significance test of the correlation coefficient used is the t-test with effective degrees of freedom.

To exclude a control variable's influence, we use partial correlation analysis to test the correlation between two variables so that the linear effects from the control variable are removed(Aloe 2014). The equation is as follows [Eq. 3]:

$$R = \frac{R_{12} - R_{13}R_{23}}{\sqrt{\left(1 - R_{13}^2\right)\left(1 - R_{23}^2\right)}} \tag{3}$$

where R_{12}、R_{13} and R_{23} represent the correlation coefficients between X_1 and X_2, X_1 and X_3, and X_2 and X_3, respectively. R represents the partial correlation coefficient between X_1 and X_2 when X_3 is the control variable.

This study uses a two-tailed Student's t-test to test the statistical significance of the linear correlation analysis between two autocorrelated series. The effective number of degrees of freedom is calculated by [Eq. 4]:

$$\frac{1}{N^{eff}} \approx \frac{1}{N} + \frac{2}{N}\sum_{j=1}^{N}\frac{N-j}{N}\rho_{XX}(j)\,\rho_{YY}(j) \tag{4}$$

where N is the sample size, $\rho_{XX}(j)$ is the autocorrelation of the series X at the time of sampling, $\rho_{YY}(j)$ is for the series Y, and j is the time lag(Li et al. 2013).

3 Results

3.1 The cross-seasonal connection between ASM and NTA SST

The NTA (0°–15°N, 80°W–10°W) is one of the crucial zones for SST variability in the Tropical Atlantic(Handoh et al. 2006). NTA SST warming typically develops in winter (DJF) and peaks in the following spring (MAM)(Bates 2008). We calculate trends and time series for global SST across four seasons (Fig. S1). Spatiotemporal patterns show that the NTA region experiences the most rapid winter warming (0.021 °C /yr, $p < 0.05$) compared to other global oceanic regions, surpassing the warming rate of the global average SST (0.011 °C /yr, $p < 0.05$) during the same period, as well as the warming rates observed in the Tropical Pacific and Indian Oceans at the same latitudes (Fig. 1). It is widely acknowledged that the increase in greenhouse gas concentrations in the atmosphere is the primary driver contributing to the overall warming in SST(Cheng et al. 2022). Therefore, internal variability may play an important role in the rapid warming trend observed in DJF NTA SST.

The Amazon rainforest, bordering the NTA, has significant impacts on internal climate variability, with frequent droughts over the past few years(Jiménez-Muñoz et al. 2016; Marengo et al. 2008, 2011). SM and Palmer Drought Severity Index (PDSI) are important indicators for monitoring

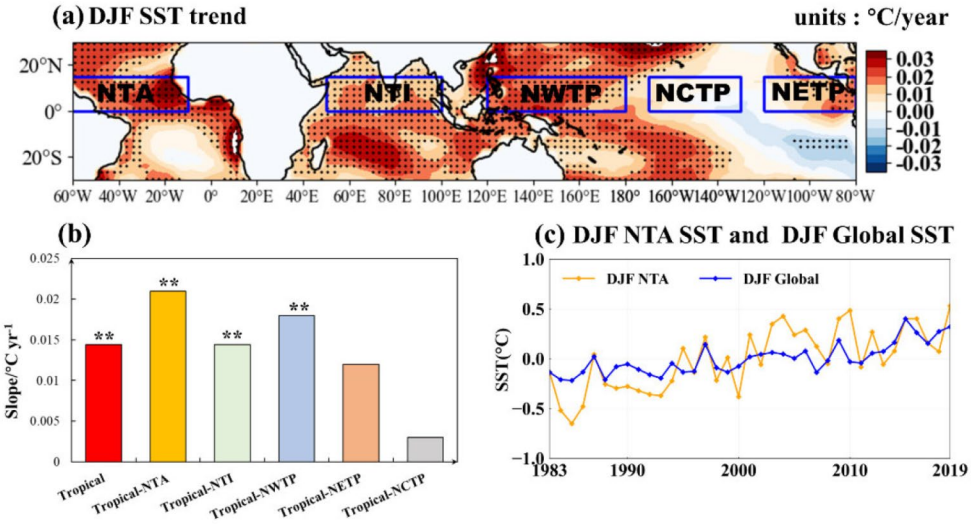

Fig. 1 Trend of NTA SST. (**a**) is the trend in observed DJF SST for the period 1983–2019. The blue boxes represent the defined NTA (0°–15°N, 80°W–10°W, regions of interest to the study), North Tropical Indian (NTI, 0°–15°N, 50°E–100°E), North Western Tropical Pacific (NWTP, 0°–15°N, 120°E–180°E), North Central Tropical Pacific (NCTP, 0°–15°N, 170°W–130°W), and North Eastern Tropical Pacific (NETP, 0°–15°N, 120°W–80°W) areas respectively. **(b)** are the trend values in observed SST (units: °C) in Tropical (0°–15°N, 0°–360°), NTA, NTI, NWTP, NETP, and NCTP for DJF in during 1983–2019. ** represent the slope is significant at $p < 0.05$. **(c)** is the global mean SST (°C) anomaly time series and DJF NTA SST (°C) anomaly time series for the period 1983–2019. The NTA SST is defined as the weighted average of SST in the regions of (0°–15°N, 80°W–10°W). The dotted shading indicates the trend is significant at the 95% confidence level

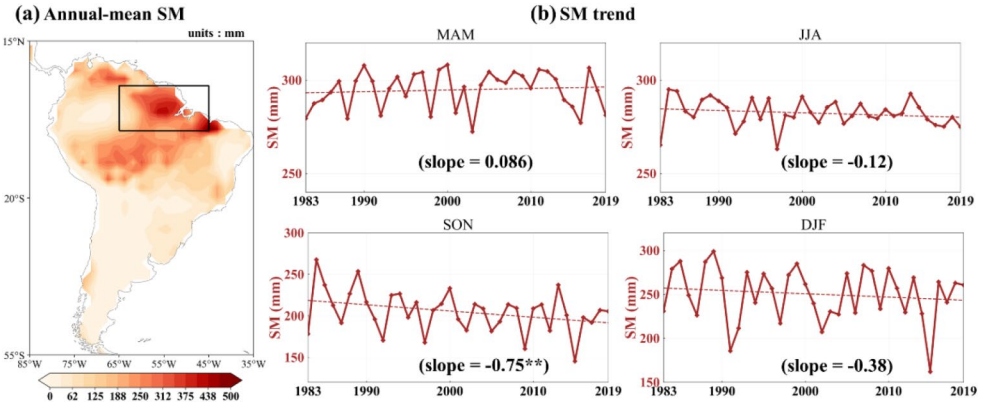

Fig. 2 Trend of ASM. **(a)** is the annual mean SM (mm) for the period 1983–2019. **(b)** is the ASM time series for MAM, JJA, SON, DJF for the period 1983–2019. The dashed red lines represent the trend. The ASM is defined as the weighted average of SM in the regions of (black box in the figure, 5°S–5°N, 65°W–45°W), respectively. ** represents slope is significant at $p < 0.05$

drought conditions(Mika et al. 2005). The soils prevalent in the Amazon region has high water content, especially over the eastern Amazon region (5°S–5°N, 65°W–45°W) (black box in Fig. 2a) with strong L-A coupling(Gerken et al. 2019). Analysis of ASM trends reveals that the Amazon region experiences a more pronounced rate of droughts during autumn (SON) compared to other seasons (Fig. 2b and Fig. S2). Furthermore, the PDSI in the Amazon also demonstrates a significant decline trend during autumn, surpassing the rates observed in other seasons (Fig. S3).

The result mentioned above highlights that the Amazon experiences the most severe drought during autumn while the adjacent NTA experiences rapid warming during the following winter. This prompts the question of whether there is connection between these two phenomena. Consequently, we compute the lead-lag correlations between DJF NTA SST and global SM. As shown in Fig. 3a the DJF NTA SST exhibits significant negative correlation with ASM in the preceding season. To further investigate this relationship, we calculate the NTA SST index and compared it with the ASM index and Amazon PDSI (APDSI) index (Fig. 3b). Bootstrap method is employed to detect whether the winter NTA SST exhibits significant differences following anomalously dry autumn soil moisture conditions over Amazon. The results indicate that when a negative anomaly occurs in autumn Amazon soil moisture, a warm anomaly typically emerges in the following winter NTA SST (Fig. 3c). The correlation coefficient between the NTA SST and ASM reaches −0.54 ($p < 0.05$), with ASM leading by one season. This relationship remains prominent ($r = -0.47$, $p < 0.05$) even after removing long-term trends. Similarly, the correlation coefficient between the NTA SST and APDSI reaches −0.52

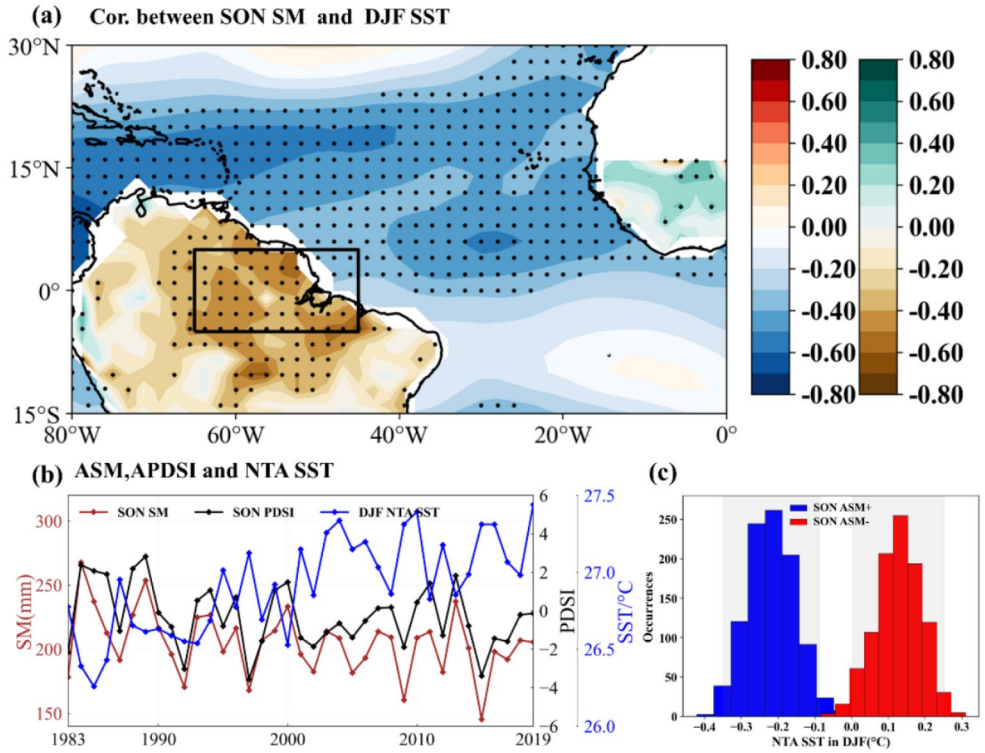

Fig. 3 Lead-lag relationship between the ASM and NTA. The detrended correlation map of the SON Amazon (black box in the figure, 5°S–5°N, 65°W–45°W) SM index with **(a)** DJF SST (blue and red color in the figure). The detrended correlation map of the DJF NTA (0°–15°N, 80°W–10°W) SST index with **(a)** SON SM (brown and green color in the figure). **(b)** is the corresponding time series of DJF NTA SST index, SON ASM index and SON APDSI index for the period 1983–2019. They are defined as the weighted average of SST in the regions of (0°–15°N, 80°W–10°W), the weighted average of SM and PDSI in the regions of (5°S–5°N, 65°W–45°W), respectively. The dotted shading indicates the correlation is significant at the 95% confidence level. **(c)** is the histogram of 10,000 realizations of the bootstrap method for the winter NTA SST anomaly indices of the preceding autumn ASM anomaly. Vertical red and blue lines indicate the mean values of 10,000 inter-realizations for the winter NTA SST index after autumn ASM dry and wet anomaly, respectively. Gray shaded regions indicate the respective doubled standard deviations (SDs; the 95% confidence interval based on the normal distribution) of the 10,000. If the gray shaded regions do not overlap each other, then the statistical significance is above the 95% confidence level

($p < 0.05$), and the relationship also remains prominent ($r = -0.48$, $p < 0.05$) after removing long-term trends. The interannual variations of NTA SST and ASM (APDSI) exhibit inversed changes from 1983 to 2019, with high SST values corresponding to low SM and PDSI values in most years. Moreover, NTA SST and ASM exhibit significant opposite trends, with NTA SST showing increasing trend and ASM showing declining trend. Employing the Pearson correlation coefficient formula, we calculate the separate contributions of ASM and NTA interannual and trend components to the observed negative correlation. The interannual component accounts for 56% of the relationship between SON ASM and DJF NTA, while the trend component contributes the remaining 44%. During the analysis period, the magnitude of the anomalous decrease in SON ASM post-2000 is larger than pre-2000. We further calculated correlation coefficients (after removing long-term trends) between SON ASM and DJF NTA SST for the two periods: pre-2000 and post-2000. The post-2000 correlation ($r = 0.38$) between SON ASM and DJF NTA SST, although weaker than the pre-2000 correlation ($r = -0.53$, $p < 0.05$), remains statistically significant. These findings underscore the robustness of the observed relationship between ASM and NTA SST, independent of the specific time period analyzed. Based on the analysis above, we may infer that the warming of DJF NTA SST is closely linked to the reduction of ASM in the preceding season. The SON Amazon drought may amplify the warming of DJF NTA SST.

Previous research indicates that the warming of NTA SST is also associated with ENSO and NAO on interannual time scales (Czaja et al. 2002). Thus, it is crucial to examine whether the NTA-Amazon connection is independent of ENSO and NAO. By employing sliding correlations, as depicted in Fig. S4, the results reveal that both concurrent and lagged relationships between ENSO, NAO, and DJF NTA SST are relatively weak compared to SON ASM. Furthermore, there is no discernible trend observed in ENSO and NAO. Specifically, there is a robust relationship between ENSO and spring NTA SST via complex air-sea coupling ENSO(Amaya and Foltz 2014; Huang 2004), but

the simultaneous relationship with the winter NTA SST is remarkably weak, suggesting that ENSO has minimal direct influence on winter NTA SST warming. Consequently, ENSO and NAO cannot account for the warming of DJF NTA SST, nor do they contribute to the warming trend of DJF NTA SST. As shown in Fig. S5, after removing the winter and autumn ENSO signal respectively, the correlation between NTA SST and ASM is still prominent ($r = -0.45$ and $r = -0.41$), thereby indicating that the NTA-Amazon connection is statistically independent of ENSO. Furthermore, after removing the winter NAO signal, the correlation between NTA SST and ASM remains prominent ($r = -0.53$), suggesting that the NTA-Amazon connection is also statistically independent of the NAO. It is worth noting that the DJF NTA SST may be influenced by SST in the preceding season due to SST persistence. The relationship between SON ASM and NTA SST is significant leading by one season, while the relationship with SON NTA SST is weak ($r = -0.28$, Fig. S6), suggesting that the changes in SON ASM are not influenced by the NTA during the same period. After removing the SON NTA SST signal, a significant correlation between NTA SST and ASM remains ($r = -0.55$). Previous studies also proposed that the positive phase of Indian Ocean Dipole (IOD) leads to westerly anomalies over the Tropical Atlantic, weakening the easterly trade winds and inducing a warm SST anomaly(Zhang and Han 2021). Nevertheless, even after removing the IOD signal, a significant correlation between NTA SST and ASM still exists ($r = -0.49$). As mentioned above, the relationship between NTA SST and ASM is shown to be independent of ENSO, NAO, IOD and SON SST, indicating a robust connection during the analyzed period. Further investigation is necessary to understand the underlying mechanisms.

3.2 The physical process associated with the influence of ASM on NTA SST

The feedback between SM and the atmosphere may play an important role in the connection between SON ASM and DJF NTA SST. SM usually has a memory of several months and is capable of retaining a wet or dry anomaly over an extended period, which is a key component of L-A interactions(Seneviratne et al. 2006). Fig. S7a and b shows the time series and correlation analysis reveal a significant correlation and consistent changes in ASM during SON and DJF ($r = 0.71$, $p < 0.05$). The ASM in DJF also showed a decreasing trend in winter. This implies that ASM anomalies in SON can persist into DJF. SM changes atmospheric circulation by affecting the land surface energy and water balance(Seo and Ha 2022). The Soil Moisture-Precipitation (SM-P) positive feedback mechanism allows the SM to persist over a certain period, and it is also an important process by which the SM influences the atmosphere(Eltahir 1998; Findell and Eltahir 1997). Fig. S7c and d demonstrate positive correlations between SM and precipitation, as well as evaporation. The decreased ASM leads to simultaneous reductions in evaporation and moisture convergence in the lower atmosphere, resulting in diminished water vapor in the atmosphere and subsequently reduced the precipitation. The soils cannot be replenished adequately by rainfall, perpetuating the decline in SM, and establishing a positive feedback loop that sustains the ASM anomaly. The positive L-A feedback mechanism played a significant role in the persistence of the ASM anomaly, which subsequently influences winter precipitation and atmospheric circulation patterns.

We calculate the lagged regression of the SON ASM with atmospheric circulation in DJF. The regression map, depicted in Fig. 4a, shows that the decrease in SON ASM leads to reduced precipitation not only over land but also over the Tropical Atlantic Ocean at the same latitude, weakening the winter Intertropical Convergence Zone (ITCZ) over the Tropical Atlantic. The decrease in SON ASM also triggers anomalous subsidence and weakening of the winter Hadley circulation across the Tropical Atlantic Ocean (Fig. 4b). This demonstrates that decreased ASM through the local L-A feedback induces alterations in the overall Tropical Atlantic atmospheric circulation. Similar findings and conclusions have been reported in previous studies. The variability of SM significantly contributes to the climate changes in tropical regions through L-A feedback(May et al. 2015). As SM decreases, surface evaporation weakens, resulting in a reduction of atmospheric relative humidity and instability, which in turn suppresses convection and upward motion(Dong et al. 2022; Liu et al. 2022). The weakened Hadley circulation further causes anomalous southwesterly winds (Fig. 4c), which weaken the background northeasterly trade winds over the Northern Hemisphere tropics. The weakened wind stress inhibits latent heat release, contributing to SST warming in the NTA region (Fig. 4d). This process aligns with the WES feedback mechanism. The SON NTA SST has a weak relationship with the winter Tropical Atlantic atmospheric circulation (Fig. S8). Therefore, the influence of SON NTA SST on the winter tropical Atlantic atmospheric circulation is not considered. As mentioned above, Hadley circulation anomalies induced by Amazon drought are critical for causing SST warming by suppressing latent heat release from the ocean via WES feedback. Previous studies have demonstrated that the key regions of land-atmosphere interaction, including the Amazon, exhibit strong land -atmosphere coupling especially in autumn(Yuan et al. 2023). The ITCZ over the NTA resides above the Amazon during winter. Therefore, a reduction in autumn Amazon soil moisture can significantly induce

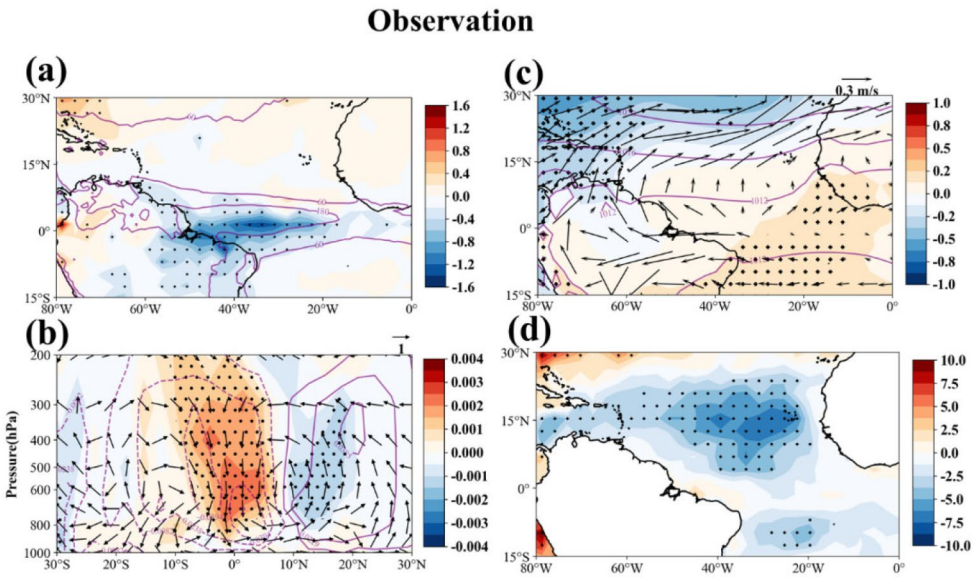

Fig. 4 The physical process of connecting ASM with NTA SST. To visualize the impact of the ASM reduction, all results are multiplied by minus one. Regression of the DJF **(a)** precipitation (units: mm/day, shading), **(b)** meridional–vertical circulation anomalies averaged between 80°W–20°W (vectors) and vertical velocity anomalies (units: Pa/s, shading), **(c)** surface pressure (units: hPa, shading) and 850 hPa wind (units: m/s, vectors), and **(d)** Latent Heat Flux (units: W/m^2, shading) with the SON ASM index for the period 1983–2019. Contours represent DJF-mean climatology. The Latent Heat Flux is defined to be positive upward. The dotted shading indicates the regression is significant at the 95% confidence level

anomalous subsidence of Hadley circulation airflow, subsequently leading to NTA SST warming through the WES feedback. In addition, we further carry out analysis by regressing sensible heat flux and net shortwave radiation onto the SON ASM index (Fig. S9). Decreased ASM causes less cloud cover over the Tropical Atlantic, allowing more solar shortwave radiation to directly reach the surface of the NTA ocean, thus leading to increased heat absorption and higher SST. The impact of sensible heat flux, however, is not significant.

3.3 Modeling evidence for the physical process of ASM-NTA SST connection

Global climate models are important tools for comprehending climate change, its causes, and future projections. The latest phase of the Coupled Model Intercomparison Project (CMIP), CMIP6, serves as a vital database for evaluating model performance in simulating historical and present climate change, as well as projecting future changes(Eyring et al. 2016). Previous researches demonstrate the CMIP6 models' ability to effectively replicate the cyclic variation characteristics of SM and the associated physical processes(Qiao et al. 2022). In this study, we further verify the lagged relationship and the physical mechanism connecting ASM and NTA SST using CMIP6 models. Fig. S10a presents the Taylor diagram illustrating the ASM-related NTA SST in CMIP6. We also calculate the correlation coefficients between the SON ASM index and DJF NTA SST index in the CMIP6 models (Fig. S10b). Among the simulation results, the ACCESS-CM2 model exhibits the highest similarity to observations, displaying both the highest correlation coefficients and the best spatial pattern correspondence between the two variables. In addition to the ACCESS-CM2, the FGOALS-g3 model also demonstrates proficiency in simulating ASM-NTA SST connection.

To comprehend the mechanism behind the SM-induced SST warming, the corresponding Hadley circulation and heat fluxes in the simulations of the CMIP6 models are analyzed. Based on the results of the model evaluation, we specifically focused on ACCESS-CM2 to examine the ASM-NTA SST connection. We examine the simulated lagged correlation between the SON ASM index and the DJF SST in ACCESS-CM2. As shown in Fig. S11a, the lagged response of the NTA SST to the SON ASM forcing remained significant. Furthermore, the model results indicates that simulated SON ASM can persist into DJF (Fig. S11b). As shown in Fig. 5a, consistent with the observation, the decreased SON ASM reduces the winter precipitation and weakens winter ITCZ across the Tropical Atlantic Ocean through the local L-A feedback. The CMIP6 models also replicate the observed anomalies in the winter Hadley circulation and sea surface heat flux (Fig. 5b and d). The decreased ASM weakens evaporation and thus reduces water vapor transport to the atmosphere, leading to a weakening of the hydrostatic instability in the troposphere, causing anomalous

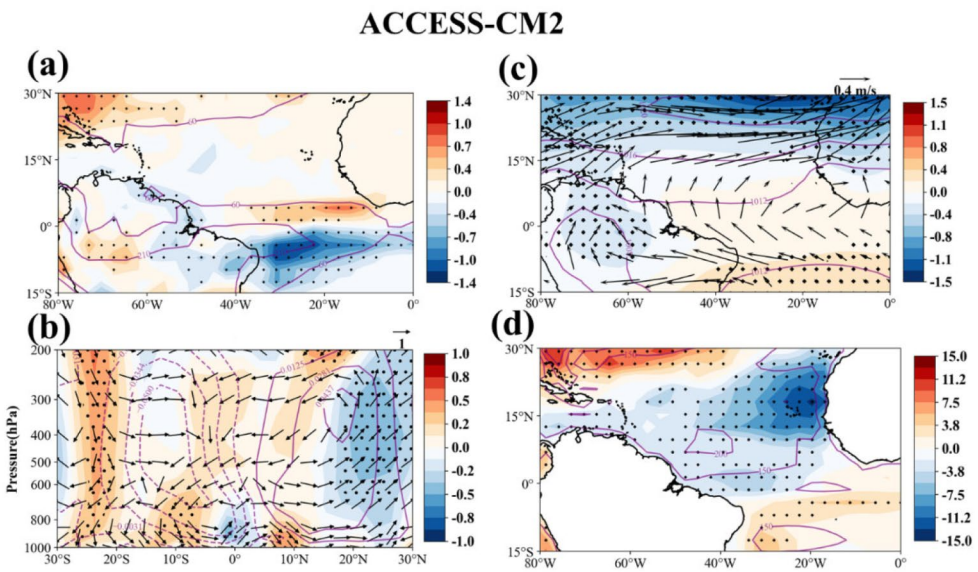

Fig. 5 is same as Fig. 4, but for the simulation results of CMIP6 model (ACCESS-CM2)

subsidence and weakening the winter Hadley circulation over the Tropical Atlantic Ocean. As a result, the weakened Hadley circulation leads to anomalous southwesterly winds in the NTA, which are opposite in direction to the northeasterly trade wind in the background flows (Fig. 5c). Consequently, sea surface evaporation is prohibited, resulting in a significant decrease in surface latent heat flux, thereby contributing to the warming of NTA SST. Our comparisons of observations and modeled data reveal consistently strong responses in precipitation and the Hadley circulation to Amazon droughts. However, a southward bias is evident, potentially linked to systematic errors in model simulations. This bias manifests as a southward shift in the simulated climatological position of the ITCZ, which is mirrored by a southward displacement of the climatological Hadley circulation. Despite exhibiting a southward bias in its mean state, the model captures the observed relationship between ASM and Hadley circulation strength (Fig. S12). In both simulation and observations, the decreased ASM leads to the weakening of the ITCZ and Hadley circulation over the tropical Atlantic. Overall, the physical mechanism reproduced in the ACCESS-CM2 aligns well with observations, providing credibility to the ASM-NTA SST connection. It is trustworthy that the physical mechanism of the ASM-NTA SST connection can be summarized as the Amazon drought weakening the Hadley circulation and further via WES effect amplifying the warming of the NTA SST.

To further validate the impact of the Amazon drought on NTA SST, we conduct sensitivity experiments by simulating the reduction of SM in Amazon using ICTPGCM model (SM_Neg, see methods) to observe changes in atmospheric circulation and SST. As shown in Fig. 6a and c, there is a significant warming of NTA SST, a significant decrease in precipitation and a weakening of the ITCZ across the Tropical Atlantic Ocean during winter, following the reduction of SM in the Amazon region. The winter movement of the Hadley circulation simulated by the model is weakened, which is manifested by a strong updraft over the north of the equator, while the south of the equator is dominated by subsidence (Fig. 6b). The weakened Hadley circulation further causes anomalous suppression of southwesterly winds, thereby inhibiting latent heat release and resulting in SST warming during DJF (Fig. 6d). These results are generally consistent with observation and CMIP6 simulations. Similar conclusions have also been reported by previous studies through experimental investigations. Tropical Amazon rainforest deforestation leads to a decrease in regional evapotranspiration and precipitation, resulting in reduced moisture convergence and diminished upward motion, thereby weakening the Hadley circulation(Gedney and Valdes 2000; McGuffie et al. 1995; Zhang et al. 1996). Consequently, it is suggested that the Amazon drought weakens the Hadley circulation over the Tropical Atlantic and amplifies the NTA SST warming.

3.4 A linear model for NTA SST warming

According to above analysis, it can be concluded that there is a strong connection between NTA SST and ASM, which is robust in both observations and model simulations. The lagged warming response of NTA SST to decreased SON ASM is noteworthy, and its underlying physical mechanism is illustrated in Fig. 7. The persistence of the SON ASM anomaly into the following season is facilitated by the positive L-A feedback, resulting in weakened ITCZ and Hadley circulation over the Tropical Atlantic Ocean in DJF. Consequently, the weakened circulation induces a southwesterly wind anomaly, which hampers evaporation and suppresses

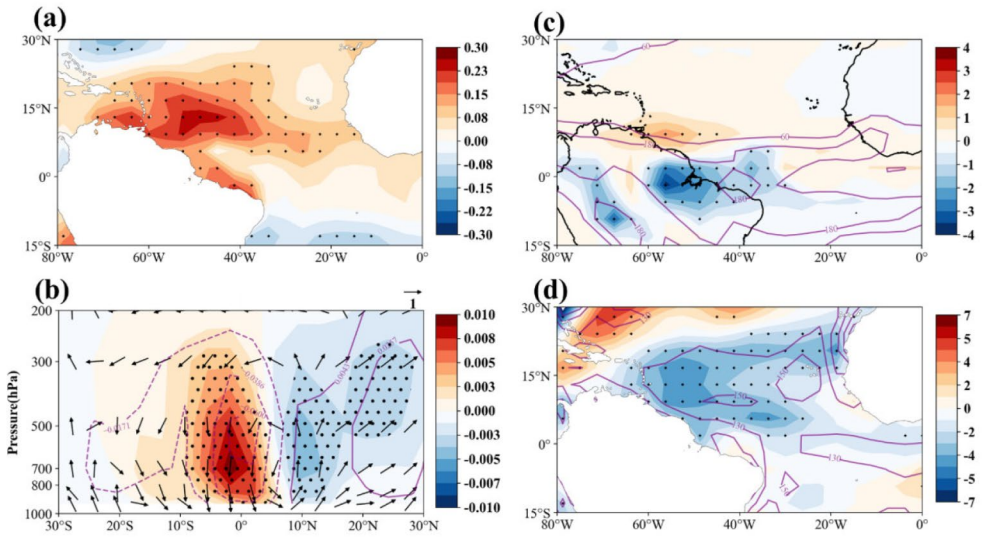

Fig. 6 Simulated results from the sensitivity experiments using ICT-PGCM model for the winter season response to the reduction of the Amazon soil moisture. **(a)** SST (units: °C, shading), **(b)** meridional–vertical circulation anomalies averaged between 80°W–20°W (vectors) and vertical velocity anomalies (units: Pa/s, shading), **(c)** precipitation (units: mm/day, shading) and **(d)** Latent Heat Flux (units: W/m^2, shading). Contours represent the DJF-mean climatology of CTRL experiment. The Latent Heat Flux is defined to be positive upward. The dotted shading indicates the regions where the results from the sensitivity simulations are significantly different from the control at the 95% confidence level

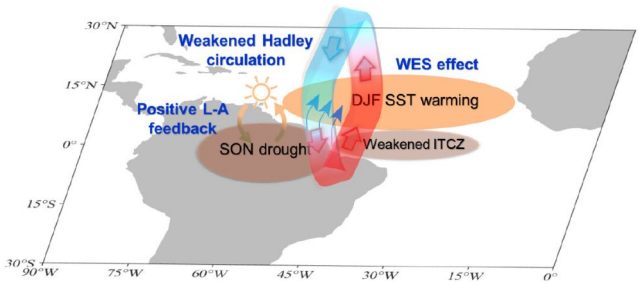

Fig. 7 Schematic of mechanisms. Schematic summarizing the impact of ASM on NTA SST as described in this study. The blue arrows are surface wind anomalies. The orange and brown gradient arrows and the sun symbol represent the feedback processes between SM and atmospheric. The red and blue circle is the SM reduced induces weakened Hadley circulation. See the main text for details of the mechanism

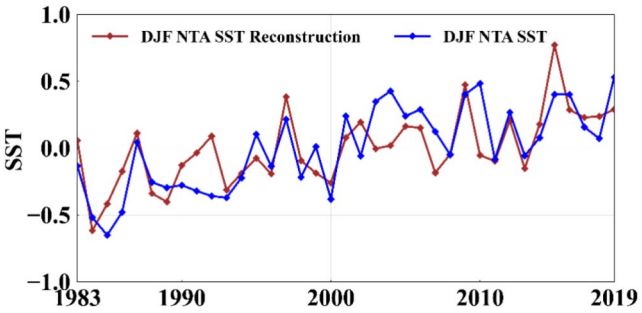

Fig. 8 Multiple Linear Regression (MLR) models constructed based on ASM. The observed (blue) and reconstructed (red) SST series (units: °C) of the NTA using the MLR method (see Methods for details) for the period 1983–2019

latent heat release, ultimately resulting in the warming of NTA SST. The WES feedback mechanism plays a role in causing the NTA SST warming. The increase in SST can be largely attributed to Global Warming (GW), as the ocean, being a significant heat reservoir, absorbs a considerable amount of heat, thereby causing a rise in SST(von Schuckmann et al. 2023). Thus, we reconstruct the yearly NTA SST series based on ASM and Global SST for the period 1983–2019 [Eq. 5]:

$$NTA_{DJF} = a * GW_{DJF} + b * ASM_{SON} + c \quad (5)$$

where a, b, and c are coefficients. The correlation coefficient between the regression result and observed series is high ($r = 0.72$, $p < 0.05$), demonstrating the strong reconstruction ability of the established multiple regression model. The reconstructed series effectively captures the peak values of NTA SST warming and corresponds well with the observation during the analysis period (Fig. 8). The trend of the reconstructed series is 0.016 °C/yr, capturing 80% of the observed NTA trend (0.021 °C/yr), with global warming contributing 2/3, and ASM contributing 1/3 of the trend. In the warming of DJF NTA SST, the external forcing factors GW have played a significant role, while among internal climate variability factors, the L-A coupling factor ASM makes a more prominent contribution than the atmospheric and oceanic factors. Furthermore, the trend of the reconstructed series is higher than the observed global average SST trend (0.011 °C/yr), suggesting that the Amazon drought does

indeed amplify NTA SST warming. We also develop a similar model that replaced GW_{DJF} in (5) with the annual mean greenhouse gas index (AGGI downloaded from https://gml.noaa.gov/aggi/aggi.html), and the contribution of ASM to the reconstructed NTA warming trend aligns well with the estimates obtained from the model using global mean SST and ASM.

4 Conclusion and discussion

The Amazon rainforest experiences severe drought during autumn, while the adjacent NTA SST exhibits the rapid rate of warming during the following winter. The relationship between the two is unclear. This study found a strong reversed relationship between the interannual variations of DJF NTA SST and SON ASM. The decreased SON ASM, which is persisted via positive L-A feedback, results in weakened ITCZ and weakened winter Hadley circulation over the Tropical Atlantic. The weakened Hadley circulation further caused a south-westerly wind anomaly over the NTA, thus weakening the trade winds, suppressing the latent heat release, and warming the NTA SST via the WES effect. Simulated CMIP6 fully coupled models and SM-forced mixed layer ocean model suggest that the Amazon drought weakens the Hadley circulation over the Tropical Atlantic and warms the NTA SST. Considering the lagged response of NTA SST to previous ASM signals, a multiple regression method is used to construct and validate a linear fitting model. The reconstructed series are in good correspondence with the observed series ($r = 0.72$), exhibiting considerable reconstruction skill for the NTA SST. The regression results also show the important contribution of Amazon drought to the rapid warming trend of NTA SST. This study not only indicates that the ASM affects warming of NTA SST through weakening the Hadley circulation and the WES mechanism, but it also shows that Amazon drought has an important impact on NTA, with Amazon drought amplifying the warming of NTA SST. Therefore, it is highly necessary to protect the Amazon rainforest.

While this study focuses on the impact of autumn Amazon drought on basin-wide NTA SST variability, highlighting the importance of thermodynamic processes, it acknowledges the potential for additional sub-basin scale processes contributing to SST warming. Notably, the elevated warming rate observed in the coastal African region suggests potential influence from internal oceanic dynamics and other processes beyond the scope of this study. Previous research has documented strong upwelling processes along the African coast (Benazzouz et al. 2014; McGregor et al. 2007). These upwelling events, driven by equatorial currents and trade winds, involve the transport of cooler, nutrient-rich subsurface waters to the surface along the eastern boundary of the tropical North Atlantic (Tomczak and Godfrey 1994). Therefore, future studies will involve more comprehensive experiments to isolate the specific roles of mixed-layer thermodynamics and internal ocean dynamics. Additionally, the CMIP6 simulated relationships of ASM with NTA SST and relevant atmospheric circulation are model dependent, and in some CMIP6 models are relatively weaker. This highlights the substantial uncertainty in the ability of models to simulate the interactions between soil moisture and large-scale atmospheric circulation. This also underscores the need for a systematic evaluation and improvement of how models represent the coupled land-atmosphere feedback processes involving Amazon land surface conditions and atmospheric circulation.

This study reveals a statistically significant year-to-year connection between SON Amazon soil moisture anomalies and the subsequent DJF NTA SST, independent of their long-term trends. Utilizing CMIP6 simulations and sensitivity experiments, we demonstrate that Amazon SM variability can influence the North Atlantic SST by modulating the Hadley circulation and the Intertropical Convergence Zone (ITCZ). These findings suggest that the Amazon-NTA SST relationship may extend beyond interannual timescales and contribute to interdecadal variations. Specifically, Amazon droughts may amplify the observed warming trend in the tropical North Atlantic. Future research should explore the potential role of large-scale multi-decadal internal climate variability, as identified in previous studies(Gomes et al. 2021; Kayano and Capistrano 2014; Tao et al. 2021; Towner et al. 2020), through additional targeted experiments. Previous studies have suggested that the Atlantic SST also has an impact on the Amazon climate(Ciemer et al. 2020; Marengo et al. 2011). The interaction and feedback between the two can be further explored in future work. Furthermore, there are discrepancies between the CMIP6 model and observational results, such as the location of reduced precipitation centers. These biases may be related to some parameters in the models or uncertainty in the models' ability to simulate atmospheric circulation. Therefore, ocean dynamic processes and the reasons for model differences should be considered in future works.

Supplementary Information The online version contains supplementary material available at https://doi.org/10.1007/s00382-024-07400-1.

Author contributions C.S., designed the research. WL, and CS, performed the data analysis, prepared all figures, and led the writing of the manuscript. All the authors discussed the results and commented on the paper.

Funding This research is supported by the National Natural Science Foundation of China (42375025, 42288101 and 41975082).

Data availability The original observational data are publicly available. All data sources are mentioned in the Materials and Methods section. The source codes for the analysis of this study are available from the corresponding author upon reasonable request. The code of ICTPGCM is available through the https://www.ictp.it/research/esp/models/speedy.aspx.

Declarations

Competing interests The authors declare that they have no competing interests.

References

Abatzoglou JT, Dobrowski SZ, Parks SA, Hegewisch KC (2018) Sci Data 5:170191. https://doi.org/10.1038/sdata.2017.191. TerraClimate, a high-resolution global dataset of monthly climate and climatic water balance from 1958–2015

Agami Reddy T (2011) Estimation of Linear Model parameters using least squares. In: Reddy TA (ed) Applied Data Analysis and Modeling for Energy Engineers and scientists. Springer US, Boston, MA, pp 141–182. doi:https://doi.org/10.1007/978-1-4419-9613-8_5

Aloe AM (2014) An empirical investigation of partial effect sizes in Meta-Analysis of Correlational Data. J Gen Psychol 141:47–64. https://doi.org/10.1080/00221309.2013.853021

Alves de Oliveira BF, Bottino MJ, Nobre P, Nobre CA (2021) Deforestation and climate change are projected to increase heat stress risk in the Brazilian. Amazon Commun Earth Environ 2:207. https://doi.org/10.1038/s43247-021-00275-8

Amaya DJ, Foltz GR (2014) Impacts of canonical and Modoki El Niño on tropical Atlantic SST. J Geophys Research: Oceans 119:777–789. https://doi.org/10.1002/2013JC009476

Amaya DJ, DeFlorio MJ, Miller AJ, Xie S-P (2017) WES feedback and the Atlantic Meridional Mode: observations and CMIP5. Comparisons Clim Dynamics 49:1665–1679. https://doi.org/10.1007/s00382-016-3411-1

Austin PC, Tu JV (2004) Bootstrap methods for developing predictive. Models Am Stat 58:131–137. https://doi.org/10.1198/0003130043277

Bates SC (2008) Coupled ocean–atmosphere Interaction and Variability in the Tropical Atlantic Ocean with and without an Annual cycle. J Clim 21:5501–5523

Benazzouz A et al (2014) On the temporal memory of coastal upwelling off NW Africa. J Geophys Research: Oceans 119:6356–6380. https://doi.org/10.1002/2013JC009559

Boulton CA, Lenton TM, Boers N (2022) Pronounced loss of Amazon rainforest resilience since the early 2000s Nature Climate Change 12:271–278 https://doi.org/10.1038/s41558-022-01287-8

Chang P, Ji L, Li H (1997) A decadal climate variation in the tropical Atlantic Ocean from thermodynamic air-sea. Interact Nat 385:516–518. https://doi.org/10.1038/385516a0

Chang P, Fang Y, Saravanan R, Ji L, Seidel H (2006) The cause of the fragile relationship between the Pacific El Niño and the Atlantic Niño. Nature 443:324–328. https://doi.org/10.1038/nature05053

Chen S, Wu R, Chen W, Hu K, Yu B (2020) Structure and dynamics of a springtime atmospheric wave train over the North Atlantic and Eurasia Climate Dynamics. 54. https://doi.org/10.1007/s00382-020-05274-7

Cheng L et al (2022) Past and future ocean warming. Nat Reviews Earth Environ 3:776–794. https://doi.org/10.1038/s43017-022-00345-1

Ciemer C, Rehm L, Kurths J, Donner RV, Winkelmann R, Boers N (2020) An early-warning indicator for Amazon droughts exclusively based on tropical Atlantic sea surface temperatures. Environ Res Lett 15:094087. https://doi.org/10.1088/1748-9326/ab9cff

Cook BI, Bonan GB, Levis S (2006) Soil moisture feedbacks to precipitation in Southern Africa. J Clim 19:4198–4206. https://doi.org/10.1175/JCLI3856.1

Czaja A, Robertson AW, Huck T (2003) The Role of Atlantic Ocean-Atmosphere Coupling in Affecting North Atlantic Oscillation Variability. In: The North Atlantic Oscillation: Climatic Significance and Environmental Impact. pp 147–172. https://doi.org/10.1029/134GM07

Czaja A, Van der Vaart P, Marshall J (2002) A diagnostic study of the role of remote forcing in tropical Atlantic variability. J Clim 15(22):3280–3290

Dai A (2011) Characteristics and trends in various forms of the Palmer Drought Severity Index during 1900–2008. J Geophys Research: Atmos 116. https://doi.org/10.1029/2010JD015541

Dong X, Zhou Y, Chen H, Zhou B, Sun S (2022) Lag impacts of the anomalous July soil moisture over Southern China on the August rainfall over the Huang–Huai River Basin Climate Dynamics 58. https://doi.org/10.1007/s00382-021-05989-1

Eltahir EAB (1998) A soil moisture–rainfall feedback mechanism: 1. Theory and observations. Water Resour Res 34:765–776. https://doi.org/10.1029/97WR03499

Enfield DB, Mayer DA (1997) Tropical Atlantic sea surface temperature variability and its relation to El Niño-Southern Oscillation. J Phys Res 102:929–945. https://doi.org/10.1029/96jc03296

Eyring V, Bony S, Meehl GA, Senior CA, Stevens B, Stouffer RJ, Taylor KE (2016) Overview of the coupled model Intercomparison Project Phase 6 (CMIP6) experimental design and organization. Geosci Model Dev 9:1937–1958. https://doi.org/10.5194/gmd-9-1937-2016

Findell KL, Eltahir EAB (1997) An analysis of the soil moisture-rainfall feedback, based on direct observations from Illinois Water Resources Research 33:725–735 https://doi.org/10.1029/96WR03756

Folland CK, Boucher O, Colman A, Parker DE (2018) Causes of irregularities in trends of global mean surface temperature since the late 19th. Century Sci Adv 4:eaao5297. https://doi.org/10.1126/sciadv.aao5297

Foltz GR, Schmid C, Lumpkin R (2013) Seasonal cycle of the mixed layer Heat Budget in the Northeastern Tropical Atlantic Ocean. J Clim 26:8169–8188. https://doi.org/10.1175/JCLI-D-13-00037.1

Gatti LV et al (2021) Amazonia as a carbon source linked to deforestation and climate change. Nature 595:388–393. https://doi.org/10.1038/s41586-021-03629-6

Gedney N, Valdes PJ (2000) The effect of amazonian deforestation on the northern hemisphere circulation and climate. Geophys Res Lett 27:3053–3056. https://doi.org/10.1029/2000GL011794

Geirinhas JL, Russo AC, Libonati R, Miralles DG, Sousa PM, Wouters H, Trigo RM (2022) The influence of soil dry-out on the record-breaking hot 2013/2014 summer in Southeast Brazil. Sci Rep 12:5836. https://doi.org/10.1038/s41598-022-09515-z

Gerken T, Ruddell BL, Yu R, Stoy PC, Drewry DT (2019) Robust observations of land-to-atmosphere feedbacks using the information flows of FLUXNET Npj. Clim Atmospheric Sci 2:37. https://doi.org/10.1038/s41612-019-0094-4

Gomes MS, Cavalcanti IFA, Müller GV (2021) 2019/2020 drought impacts on South America and atmospheric and oceanic influences. Weather Clim Extremes 34:100404. https://doi.org/10.1016/j.wace.2021.100404

Gore M, Abiodun BJ, Kucharski F (2020) Understanding the influence of ENSO patterns on drought over southern Africa using. SPEEDY Clim Dynamics 54:307–327. https://doi.org/10.1007/s00382-019-05002-w

Ham Y-G, Kug J-S, Park J-Y, Jin F-F (2013) Sea surface temperature in the north tropical Atlantic as a trigger for El Niño/

Southern Oscillation. Events Nat Geoscience 6:112–116. https://doi.org/10.1038/ngeo1686
Handoh IC, Matthews AJ, Bigg GR, Stevens DP (2006) Interannual variability of the tropical Atlantic independent of and associated with ENSO: part I. North Trop Atl Int J Climatology 26:1937–1956. https://doi.org/10.1002/joc.1343
Hersbach H et al (2020) The ERA5 global reanalysis Quarterly. J Royal Meteorological Soc 146:1999–2049. https://doi.org/10.1002/qj.3803
Huang B (2004) Remotely forced variability in the tropical Atlantic. Ocean Clim Dynamics 23:133–152. https://doi.org/10.1007/s00382-004-0443-8
Huang B et al (2017) Extended reconstructed Sea Surface temperature, Version 5 (ERSSTv5): upgrades, validations, and Intercomparisons. J Clim 30:8179–8205. https://doi.org/10.1175/JCLI-D-16-0836.1
Huo L, Guo P, Hameed SN, Jin D (2015) The role of tropical Atlantic SST anomalies in modulating western North Pacific tropical cyclone genesis. Geophys Res Lett 42:2378–2384. https://doi.org/10.1002/2015GL063184
Jiang L, Li T (2019) Relative roles of El Niño-induced extratropical and tropical forcing in generating Tropical North Atlantic (TNA). SST Anom Clim Dynamics 53:3791–3804. https://doi.org/10.1007/s00382-019-04748-7
Jiménez-Muñoz JC et al (2016) Record-breaking warming and extreme drought in the Amazon rainforest during the course of El Niño 2015–2016. Sci Rep 6:33130. https://doi.org/10.1038/srep33130
Jin D, Huo L (2018) Influence of tropical Atlantic sea surface temperature anomalies on the east Asian summer monsoon Quarterly. J Royal Meteorological Soc 144:1490–1500. https://doi.org/10.1002/qj.3296
Kayano MT, Capistrano VB (2014) How the Atlantic multidecadal oscillation (AMO) modifies the ENSO influence on the south American rainfall International. J Climatol 34:162–178. https://doi.org/10.1002/joc.3674
Krzywinski M, Altman N (2015) Multiple linear regression. Nat Methods 12:1103–1104. https://doi.org/10.1038/nmeth.3665
Kucharski F, Molteni F, Yoo JH (2006) SST forcing of decadal Indian Monsoon rainfall variability Geophysical. https://doi.org/10.1029/2005GL025371. Research Letters 33 doi
Kucharski F et al (2016) The teleconnection of the Tropical Atlantic to Indo-Pacific Sea Surface temperatures on inter-annual to Centennial Time scales: a review of. Recent Find Atmos 7:29. https://doi.org/10.3390/atmos7020029
Lejeune Q, Davin EL, Guillod BP, Seneviratne SI (2015) Influence of amazonian deforestation on the future evolution of regional surface fluxes, circulation, surface temperature and precipitation. Clim Dyn 44:2769–2786. https://doi.org/10.1007/s00382-014-2203-8
Levine PA, Randerson JT, Chen Y, Pritchard MS, Xu M, Hoffman FM (2019) Soil moisture variability intensifies and prolongs eastern Amazon temperature and Carbon Cycle response to El Niño–Southern Oscillation. J Clim 32:1273–1292. https://doi.org/10.1175/JCLI-D-18-0150.1
Li J, Sun C, Jin F-F (2013) NAO implicated as a predictor of Northern Hemisphere mean temperature multidecadal variability. Geophys Res Lett 40:5497–5502. https://doi.org/10.1002/2013GL057877
Liu W, Zhang Q, Li C, Xu L, Xiao W (2022) The influence of soil moisture on convective activity: a review. Theoret Appl Climatol 149:221–232. https://doi.org/10.1007/s00704-022-04046-z
Marengo JA et al (2008) The Drought of Amazonia in 2005. J Clim 21:495–516. https://doi.org/10.1175/2007JCLI1600.1
Marengo JA, Tomasella J, Alves LM, Soares WR, Rodriguez DA (2011) The drought of 2010 in the context of historical droughts in the Amazon region Geophysical. https://doi.org/10.1029/2011GL047436. Research Letters 38 doi:
May W, Meier A, Rummukainen M, Berg A, Chéruy F, Hagemann S (2015) Contributions of soil moisture interactions to climate change in the tropics in the GLACE–CMIP5 experiment. Clim Dyn 45:3275–3297. https://doi.org/10.1007/s00382-015-2538-9
McGregor HV, Dima M, Fischer HW, Mulitza S (2007) Rapid 20th-Century increase in Coastal Upwelling off. Northwest Afr Sci 315:637–639. https://doi.org/10.1126/science.1134839
McGuffie K, Henderson-Sellers A, Zhang H, Durbidge TB, Pitman AJ (1995) Global climate sensitivity to tropical deforestation global. Planet Change 10:97–128. https://doi.org/10.1016/0921-8181(94)00022-6
Mika J, Horváth S, Makra L, Dunkel Z (2005) The Palmer Drought Severity Index (PDSI) as an indicator of soil moisture Physics and Chemistry of the Earth. Parts A/B/C 30:223–230. https://doi.org/10.1016/j.pce.2004.08.036
Nobre CA, Obregón GO, Marengo JA, Fu R, Poveda G (2009) Characteristics of Amazonian Climate: Main Features. In: Amazonia and Global Change. pp 149–162. https://doi.org/10.1029/2009GM000903
Nobre CA, Sampaio G, Borma LS, Castilla-Rubio JC, Silva JS, Cardoso M (2016) Land-use and climate change risks in the Amazon and the need of a novel sustainable development paradigm Proceedings of the National Academy of Sciences 113:10759–10768 doi:https://doi.org/10.1073/pnas.1605516113
Qiao L, Zuo Z, Xiao D, Bu L (2021) Detection, attribution, and future response of global soil moisture in summer. Front Earth Sci 9. https://doi.org/10.3389/feart.2021.745185
Qiao L, Zuo Z, Xiao D (2022) Evaluation of Soil moisture in CMIP6 simulations. J Clim 35:779–800. https://doi.org/10.1175/JCLI-D-20-0827.1
Rugg A, Foltz GR, Perez RC (2016) Role of mixed Layer dynamics in Tropical North Atlantic Interannual Sea Surface temperature variability. J Clim 29:8083–8101. https://doi.org/10.1175/JCLI-D-15-0867.1
Saji NH, Goswami BN, Vinayachandran PN, Yamagata T (1999) A dipole mode in the tropical. Indian Ocean Nat 401:360–363. https://doi.org/10.1038/43854
Sen PK (1968) Estimates of the regression coefficient based on Kendall's tau. J Am Stat Assoc 63:1379–1389. https://doi.org/10.1080/01621459.1968.10480934
Seneviratne SI et al (2006) Soil moisture memory in AGCM Simulations: analysis of Global Land–Atmosphere Coupling experiment (GLACE). Data J Hydrometeorology 7:1090–1112. https://doi.org/10.1175/JHM533.1
Seneviratne SI et al (2010) Investigating soil moisture–climate interactions in a changing climate: a review. Earth Sci Rev 99:125–161. https://doi.org/10.1016/j.earscirev.2010.02.004
Seo Y-W, Ha K-J (2022) Changes in land-atmosphere coupling increase compound drought and heatwaves over northern East Asia Npj. Clim Atmospheric Sci 5:100. https://doi.org/10.1038/s41612-022-00325-8
Song YM, Wang ZF, Qi LL, Huang AN (2019) Soil moisture memory and its effect on the Surface Water and Heat fluxes on Seasonal and Interannual Time scales. J Geophys Research: Atmos 124:10730–10741. https://doi.org/10.1029/2019JD030893
Sun C, Kucharski F, Li J, Jin F-F, Kang I-S, Ding R (2017) Western tropical Pacific multidecadal variability forced by the Atlantic multidecadal oscillation. Nat Commun 8:15998. https://doi.org/10.1038/ncomms15998
Tao L, Liang XS, Cai L, Zhao J, Zhang M (2021) Relative contributions of global warming, AMO and IPO to the land precipitation variabilities since 1930. s Clim Dynamics 56:2225–2243. https://doi.org/10.1007/s00382-020-05584-w
Tomczak M, Godfrey JS (1994) CHAPTER 4 - Ekman layer transports, Ekman pumping and the Sverdrup balance. In:

Tomczak M, Godfrey JS (eds) Regional Oceanography. Pergamon, Amsterdam, pp 39–51. doi:https://doi.org/10.1016/B978-0-08-041021-0.50008-4

Towner J, Cloke HL, Lavado W, Santini W, Bazo J, Coughlan de Perez E, Stephens EM (2020) Attribution of Amazon floods to modes of climate variability. Rev Meteorological Appl 27:e1949. https://doi.org/10.1002/met.1949

von Schuckmann K et al (2023) Heat stored in the Earth system 1960–2020: where does the energy go? Earth Syst Sci Data 15:1675–1709. https://doi.org/10.5194/essd-15-1675-2023

Wang C (2004) ENSO, Atlantic Climate Variability, and the Walker and Hadley Circulations. In: Diaz HF, Bradley RS (eds) The Hadley Circulation: Present, Past and Future. Springer Netherlands, Dordrecht, pp 173–202. doi:https://doi.org/10.1007/978-1-4020-2944-8_7

Wang C, Enfield DB, Lee S-k, Landsea CW (2006) Influences of the Atlantic Warm Pool on Western Hemisphere Summer Rainfall and Atlantic Hurricanes. J Clim 19:3011–3028. https://doi.org/10.1175/JCLI3770.1

Yang L, Sun G, Zhi L, Zhao J (2018a) Negative soil moisture-precipitation feedback. dry wet Reg Sci Rep 8:4026. https://doi.org/10.1038/s41598-018-22394-7

Yang Y, Xie S-P, Wu L, Kosaka Y, Li J (2018b) ENSO forced and local variability of North Tropical Atlantic SST: model simulations and biases. Clim Dyn 51:4511–4524. https://doi.org/10.1007/s00382-017-3679-9

Yuan R, Li F, Ye R (2023) Global diagnosis of land–atmosphere coupling based on water isotopes. Sci Rep 13:21319. https://doi.org/10.1038/s41598-023-48694-1

Zhang L, Han W (2021) Indian Ocean Dipole leads to Atlantic Niño. Nat Commun 12:5952. https://doi.org/10.1038/s41467-021-26223-w

Zhang H, Henderson-sellers A, Mcguffie K (1996) Impacts of Tropical Deforestation. Part II: The Role of Large-Scale Dynamics. J Clim 9:2498–2521